Hofmeister, R.; Floeser, G.; Schartau, M.:

Estuary-type circulation as a factor sustaining horizontal nutrient gradients in freshwater-influenced coastal systems

In: Geo-Marine Letters (2015) Springer

DOI: 10.1007/s00367-016-0469-z

Estuarine circulation sustains horizontal nutrient gradients in freshwater-influenced coastal systems

Richard Hofmeister[a,b], Götz Flöser[a], Markus Schartau[c]

[a] *Helmholtz-Zentrum Geesthacht, Institute of Coastal Research*
[b] *University of Hamburg, Institute of Hydrobiology and Fisheries Science*
[c] *GEOMAR Helmholtz Centre for Ocean Research, Kiel*

Abstract

Horizontal gradients of nutrients and suspended particulate matter (SPM) near the coast are observed and often attributed to matter input by rivers. But measurements in the southern North Sea show nutrient gradients everywhere along the coast, even without considerable river runoff. The conceptual model of the nutrient cycle in the Wadden Sea from Ebenhöh et al. (2004) is extended here with a numerical model such that key processes for the transport of particulate matter can be identified. The coastal nutrient gradient is maintained by an interplay of tidal mixing, density gradients and possibly atmospheric deposition. Similar to Ebenhöh et al. (2004), we find that shallowness is an important factor controlling relevant processes in the coastal suspended matter regime. Increasing precipitation, and most effectively higher sinking velocities of SPM enhance the horizontal nutrient gradients and eutrophication of the simulated North Sea regime, while these gradients are reversed for evaporation-dominated inverse estuaries. The simulation of coastal nutrient budgets in tidal systems thus requires to resolve the freshwater budget and tidal mixing asymmetries. The nutrients budget also indicates, that 10 % of the amount of organic carbon export into the deeper North Sea sediments may be transported towards the North Sea coast by estuarine circulation.

Key words: estuarine circulation, nutrient gradients, residual transport

1. Introduction

The coastal nutrient gradients are typically observed with and related to river runoff from the coast. Nevertheless, nutrient gradients are also present in areas without considerable riverine volume fluxes (Ebenhöh et al. (2004)).

In this study, we analyse the processes of estuarine circulation as a combination of gravitational circulation and tidal straining (see Burchard and Hetland (2010)). These processes evolve from horizontal gradients of vertically mean density in the coastal sea. The gravitational circulation forces a vanish of internal pressure gradients in the coastal system while denser water flows below lighter water. When periodically changing currents are present, such as tidal motions, the asymmetry in vertical mixing through periodically changing vertical stratification creates a mean residual flow as identified by Jay and Musiak (1994). The

presence of estuarine circulation is traced in the shallow, tidal North Sea in measurements of current profiles (Flöser et al. (2013)) and microstructure profiling (Becherer et al. (2011)). In estuarine and coastal systems in humid climate, the implied circulation heads towards the river mouth or coast near the sea bed and towards open sea near the surface. Burchard et al. (2008) proposed a theory for accumulation of suspended matter at the coast due to the residual estuarine circulation. Similarly, we will run an ecosystem model and estimate the effect of particular matter accumulation at the coast, which determines the coastal nutrient cycles. Although Cloern (1987) found that turbidity is a major control for primary productivity, the coastal nutrient gradients may not be a result of horizontally varying productivity.

The present study follows the concept of Ebenhöh et al. (2004), that shallowness produces gradients of dissolved nutrients in coastal systems. In their study, an influx of particulate organic matter is balanced by a diffusive outflow of dissolved nutrients for a given nutrient gradient. Similarly, Grunwald et al. (2010) also use a given advective influx of organic matter to get lateral nutrient gradients. They show a clear nutrient gradient with higher concentrations of silica in shallower areas throughout the year at the Spiekeroog pile, whereas phosphate and nitrate have a vanishing DIN/DIP gradient in winter. We can confirm this in section 2 with lateral measurements in the east-frisian wadden sea. The key process creating those gradients is potentially the estuarine circulation rather than advective processes within the sediment.

We will investigate analogously an opposite density gradient as present in arid systems (Gräwe et al. (2010); Hetzel et al. (2013)), where by theory then particulate matter is transported away from the coast.

Following the concept of Ebenhöh et al. (2004), also laterally homogeneous fluxes of nutrients would build up gradients in dissolved nutrients. Atmospheric deposition of nutrients (cite somebody) through aerosols, dust and rain is thus a source of nutrient gradients and is conceptually analysed in section 3.5 using a mean deposition rate from simulations (Dentener et al. (2006)).

Remineralisation under suboxic conditions in or near the sea floor removes nitrogen due to denitrification and counteracts eutrophication during import conditions of organic matter in coastal areas (Deek et al. (2013)). On the other hand, phosphate is bound to iron-hydroxides (Delaney (1998)) within the upper sediment and also in suspended matter (Lucotte and D'Anglejan (1983)), which affects the observable budget of inorganic phoshorus. Similarly, advective ground water fluxes of high nutrient concentrations originating from near coast soil (Burnett et al. (2003)) would effectively increase nutrient gradients. The local contributions of ground water fluxes can exceed contributions of rivers (Wu et al. (2013)) and therefore might be a major factor for coastal nutrient gradients.

Grunwald et al. (2010) and Ebenhöh et al. (2004) recall sea bed bound transport of organic matter, by straining transport of organic fluffy layer material (Fettweis et al. (2010)) or morphodynamic processes due to settling and scour lag (Pritchard and a.J. Hogg (2003)).

In the present study on effects of waterbody transport of organic matter, the mean cumulative effect of denitrification, binding of phosphate, ground water fluxes and morphodynamics of organic sediments are

neglected in the scenarios to focus only on the estuarine circulation.

2. Methods

2.1. Nutrient measurements

[Figure 1 about here.]

During a research cruise in summer 2005 in the German coastal waters, ammonia und orthophosphate concentrations were determined by a newly developed sequential injection system that reduced the reaction time to less than 60 s (see figure 5). The ammonium determination is based on the reaction of o-phthaldialdehyde with sodium sulphite and ammonium to a fluorescent product, while the phosphate reaction uses potassium molybdate as a reacting reagent. The fast reaction times were achieved by automation and miniaturizing the entire detection system from sample filtration to optical detection. Detection limits were 0.06 μM for ammonium and 0.05 μM for phosphate determination. Further details can be found in Frank et al. (2006).

Water samples from the Wadden Sea channels south of Langeoog Island area were taken at fixed stations during the year 2003 along a transect from the mainland (Accumersiel) towards the tidal inlet Accumer Ee (the positions are denoted by black markers in figure 5). Measuring intervals were one week in summer and two weeks in winter. Nitrate, nitrite, ammonia, silicate and dissolved orthophosphate concentrations were determined using the procedure described by Grasshoff et al. (1999).

2.2. Model description

We used an idealised model setup for near-shore coastal processes at an arbitrary coast. The model grid is aligned perpendicular to the shoreline with only one active grid point in along-coast direction. Alongshore, horizontal gradients of internal quantities are neglected in the setup such that along-shore transports leave the model state unaffected. Still, along-shore transports can be accelerated due to winds or earth rotation and feed back into the dynamics by shear production. The model GETM is used here, which is a baroclinic, hydrodynamic model, that solves the shallow-water, primitive equations. The model is linked to the GOTM turbulence module and runs a k-ε-model for the varying water depths and density stratification. A depth-adaptive, vertical grid of 20 sigma layers is used, which resolves vertical gradients of tracers and current speed even in very shallow waters.

[Figure 2 about here.]

Wind effects are included in the model in two different setups: A) currents are accelerated along and across the transect and a local wave field is formed depending on wind velocity and depth, and B) that the wind field is used to calculate the wave-stress at the sea bed only. Meteorological forcing is used from REMO simulations (Feser et al. (2001)) for a central location in the German Bight and for the year 2003.

Salinity at the open boundary is set to 33 g/kg, whereas temperature follows an idealised sinusodial, annual evolution. Other tracers are treated with a zero-gradient condition across the open boundary. A tide is imposed at the open boundary through idealistically varying sealevels with a tidal amplitude of 1 m and a period of 12 h.

Organic substances and biologically induced fluxes of nitrogen and carbon are resolved with a biogeochemical model component. For our study we apply a refined version of the Carbon- and Nitrogen Regulated Ecosystem Model (CN-REcoM) described in Schartau et al. (2007). The model distinguishes between five major compartments: nutrients, phytoplankton, zooplankton, extracellular organic matter, and detritus. Dissolved inorganic nitrogen (DIN) is the only limiting nutrient resolved. Apart from zooplankton biomass, all organic compartments vary in carbon and nitrogen content, i.e. variable carbon-to-nitrogen (C:N) ratios. Instant homeostasis is assumed for the zooplankton i.e. C:N ratio remains fixed at ... and C:N variations of assimilated phytoplankton prey are instantly compensated either by C respiration or by N excretion (e.g. urea). The phytoplankton's carbon-specific chlorophyll *a* content varies with nutrient availability and with the photoacclimation state of the algae, which is parameterised as in Geider et al. (1998).

For our model approach we introduced a logistic function for the reduction of chlorophyll *a* synthesis as soon as cellular chlorophyll-to-nitrogen ratio reaches a prescribed maximum value, for example under light-limited and nutrient replete conditions. Photosynthesis is slowly downregulated when phytoplankton growth becomes nutrient limited and the cellular N:C quota approaches a prescribed minimum subsistence quota. But C fixation may continue in spite of severe N limitation, which leads to an increase in the phytoplankton C:N ratio much higher than Redfield C:N=6.625 (106:16).

The pool of extracellular organic matter is split up into three fractions: dissolved polysaccharides (dCCHO), carbon-rich acidic transparent exopolymer particles (TEP) (CITATION FOR TEP), and a residual fraction of unspecified labile dissolved organic carbon (DOC). Both dCCHO and residual DOC are exuded by phytoplankton. A refractory fraction of DOC is disregarded in our model. Exudation and leakage of C are assumed to be proportional to phytoplankton C biomass. Maximum exudation of DOC and dCCHO by phytoplankton occurs immediately after nutrient depletion limits growth. The dCCHO fraction is subject to coagulation and forms 'acidic' macro-gels, mainly measured as stained acidic TEP. For the aggregation of dCCHO and TEP we adopted parameter values of (Engel et al., 2004). Zooplankton grazing is parameterised with a Holling Type III function, for which the grazing rate increases linearly with prey abundance at some threshold phytoplankton concentration. The zooplankton's assimilation of prey becomes saturated at high phytoplankton concentration, which is specified by a fixed maximum grazing rate. A quadratic loss term for zooplankton accounts for the net effect of higher trophic levels. This term is treated as a closure term and feeds into the detritus compartement. Detritus as well as dissolved organic nitrogen (DON) are remineralised, describing the mass flux of organic N back to DIN.

In the present study, we use the Framework for Aquatic Biogeochemical Models (FABM, Bruggeman and Bolding (2014) for coupling an the ecosystem model with a 1-size-class model for lithogenic, suspended particular matter(SPM), similar to Burchard et al. (2004). The SPM model solves an advection and diffusion equation for the volume concentration of SPM with a constant sinking velocity w_s. Additionally, a pool of particular matter along the sea bed is resolved. Fluxes of particular matter between water column and a sediment layer are possible due to erosion and sedimentation as described in Burchard et al. (2004). The photosynthetically available radiation (PAR) is attenuated by the biological and lithogenic particles in the system with an attenuation coefficient proportional to the concentration of suspended particulate matter with the factor k_d^{SPM}. The model parameters are described in table 1

Erosion in shallow waters is highly influenced by wave stress at the sea bed (Stanev et al. (2008); Puls et al. (2011)). In the present model setup, we use the combination of wind and wave stress for erosion as proposed by Soulsby (1997). The wave height and period are parameterised in dependence of wind speed (Soulsby (1997)). The present setup of wave coupling has been successfully applied in SPM modelling (Gayer et al. (2006); van der Molen et al. (2009)).

[Table 1 about here.]

3. Results and Discussion

3.1. Tidally mean structure of the flow

The tidal currents dominate the flow conditions with currents of about 1 m/s and a vertical gradient due to bottom friction like described in Jay and Musiak (1994). Although the horizontal volume flux averages out within a tidal period, the tidal mean currents show a characteristic pattern in the simulation as shown for two days of the annual simulation in figures 3 and 4, that are characterized by low wind speeds. The mean currents are directed towards the coast near the sea bed and away from the coast at the surface. Following the concept of Jay and Musiak (1994), the horizontal gradient in water density, that is mainly determined by salinity (figure 3), supports vertical mixing during flood currents and suppresses vertical mixing by stable stratification during ebb currents. The Simpson number Si, which is the ratio between stabilising effects of horizontal gradients ad tidal mixing (Stacey et al. (2010)), amounts to $5.6{\cdot}10^{-1}$ in the center of the transect throughout the simulation period. This is below the critical value of about unity, where the water body gets stratified and therefore can be considered for strain-induced periodically stratification (SIPS) with the tide (Simpson et al. (1990)). A typical transect for the dissolved nutrients is show in figure 4 with a steep increase of concentrations close to the coast (similarly to Ebenhöh et al. (2004)). The nutrient gradients in the present setup are created by the residual current near the sea bed, that transports particulate organic matter towards the coast. A detailed analysis of the effect of the density-driven, residual currents follows in section 3.3.

[Figure 3 about here.]

[Figure 4 about here.]

3.2. Increased light limitation towards the coast?

The density-driven, residual currents transport SPM towards the coast. The local dissolved concentration is not depending on accumulation only, but is also determined by effective erosion. The horizontal gradient of vertically averaged SPM is shown in figures 3 and 4 together with the vertically averaged photosynthetically available radiation.

The SPM concentrations increase steadily towards the coast, while the gradient is stronger in July than in September. The stronger horizontal density gradients in spring, that result from a combined effect of differential warming and differential freshening due to rain, is most effectivly pumping SPM towards the coast. This explanation is supported by the annual timeseries of the horizontal gradients in section 3.3.

Tidal mixing suppresses vertical stratification throughout the year in the current simulation as typically for energetic estuaries with Simpson numbers (Geyer and MacCready (2014)). The phytoplankton cells are thus present in all depths of the water column and light availability depends on depth as well as turbidity. Figures 3 and 4 show that light availability increases with decreasing water depth and increasing amount of suspended matter. In the present simulation, phytoplankton is not more limited in light in the high-turbidity waters near the coast compared to deeper areas. In fact, the results show even a minimum at 35 km off the coast. The coastal nutrient gradient is therefor not a result of increasing turbidity towards the coast.

3.3. Seasonality of nutrient concentrations and the horizontal nutrient gradient

As shown in van Beusekom et al. (2009), the nutrient concentrations are low throughout summer close to List on the island of Sylt whereas the map in 5 suggest increasing nutrient concentrations towards the very shallow parts of the bay.

[Figure 5 about here.]

Figure 5 shows measured nutrients along short transects near the coast. Observed transects are shown here, when salinity varies by 0.4 PSU. The transects without a salinity gradients are assumed to be mixed horizontally by a bay-scale event, such as a storm, and typically also do not show a nutrient gradient. The given transect profiles indicate a salinity increase with increasing latitude together with decreasing nutrient concentrations for both, dissolved inorganic nitrogen and silicate. The higher nutrient concentrations are observed in winter, while the lower concentrations are observed in early summer. The measurements from the cruises in 2003 and 2005 indicate a horizontal nutrient gradient under horizontal density gradients. While in the summer scenario in 2005, the differential warming of the coastal waters enforces the lateral density gradients, figure 5 suggests that nutrient gradients are observed throughout the year. Differential cooling

and reduced precipitation in winter reduces coastal density gradients, and thus a slower accumulation of nutrients near the coast.

The effect of freshwater supply due to rain and diffusive groundwater input on the coastal nutrient gradients is studied here in a set of four scenarios. According to Onken and Riethmüller (2010), we assume a humid freshwater flux of 2mm/day. A realistic scenario with 2mm/day freshwater flux and realistic wind stress forcing, an idealistic scenario with 2mm/day freshwater flux without wind stress forcing, a scenario without density forcing, but resolving the temperature evolution and meteorological fluxes and a scenario of an inverse estuary with a net evaporation of 2mm/day and including the full meteorological forcing. Nutrient fluxes due to sedimentation, atmospheric deposition, pore-water supply and denitrification are assumed to level out in the base scenarios. In section 3.5, the effect of a residual vertical boundary flux of nutrients is investigated.

[Figure 6 about here.]

The main driver in the dynamics of horizontal gradients in figure 6 is the seasonally varying density gradient. In the humid forcing scenarios (A,B), this density gradient is mainly created due to differential freshening by rain overlayed by the differential warming effect. In summer, the effect of lower salinities and higher temperatures near the coast shows an enhanced horizontal density gradient, whereas the cooling in autumn minimises the density gradient by colder water near the coast than offshore. The density gradient translates into SPM gradient dynamics such that an increased gradient of density increases SPM gradients. For low density gradients, the horizontal SPM gradient is more determined by erosion and sedimentation processes. The realistic scenarios shows, that for winter conditions, the horizontal transport of SPM is balanced with the sedimentation, such that the gradient stays constant. The horizontal nutrient gradient shows a negative spring peak, since the bloom starts in the shallow waters with higher temperatures and higher light availability. After the spring bloom, the gradient is vanished and starts to build up in summer to values higher than at the beginning of the year. The accumulation of nutrients could be balanced by sedimentation and denitrification near the coast.

The scenario with vanished density gradients in the dynamic equations shows a more or less constant SPM and nutrient gradient with slightly lower values of SPM and nutrients at the coast. This is due to lower current speeds in the shallow waters and more sedimentation for SPM and decelerated remineralisation in colder temperatures in winter for nutrients.

In the arid scenario (D), the density gradient is directed opposite to the humid scenarios (A,B). The estuarine circulation then is reversed, which results in decreasing SPM concentrations at the coast compared to offshore values. Similarly, nutrient gradients are reversed and enhanced with a lower level of dissolved nutrients compared to offshore waters.

The weak observed gradients in winter can be interpreted as result of event-driven horizontal mixing. The sudden, advective matter exchange in a storm event within a tidal bay cannot be represented with the transect model as used in this study. However, the high nutrient concentrations near the coast are an indicator for the amount of organically accumulated nutrients throughout the year, that are remotely supplied through the bigger non-local rivers and the North Sea water body.

3.4. Organic matter budget depending on transport

The gradients analysis suggests an increasing budget of particulate matter at the coast, if horizontal density gradients are present. In figure 7, the total mass budget for up to 30 km distance from the coast is shown. Total nitrogen and total organic nitrogen (phytoplankton, zooplankton, detritus and dissolved organic matter) are integrated as pelagic components, whereas lithgenic particulate matter is integrated as sum of suspended and sedimented mass. The available nitrogen is bound fully in the organic pool over summer. At the beginning of the spring bloom, approximately half of the nitrogen is available as dissolved inorganic nutrients, which is in accordance with Van Engeland et al. (2010) for their station TC.

[Figure 7 about here.]

Scenario C shows that for negative gradients of dissolved nutrients and SPM concentrations (compare figure 6), the total buget stays constant throughout the year and the gradients are produced by local effects rather than transport effects.

The nutrient and nitrogen budget in the humid scenarios (A,B) increases over summer during the period of strong horizontal density gradients. The mass budget of nitrogen increases in the realistic simulation by more than 5 % per simulation year. The result might be read such that if 5% of the pelagic nitrogen can be removed in coastal sediments, an established nutrient gradient would remain. The lithogenic particulate matter increases by approximately 100 kg per meter coastline in the realistic scenario. As a result of only estuarine circulation in an idealised coastal sea, this value is not relevant for observable morphodynamic changes near the coast. The estuarine circulation effectively acts against horizontal mixing of wave-eroded SPM from shallow waters to the open sea. A river at the coast, or a constriction towards the open sea by islands are subject to first order changes of the mass budget dynamics. Nevertheless, the concept of mass transport by estuarine circulation is a general feature of all types of coasts that show a horizontal density gradient.

3.4.1. Carbon budget

The transport of organic carbon is resolved by the ReCOM model and enables an analysis of the particulate and dissolved organic carbon (POC and DOC respectively) budget and the transformation of organic carbon to inorganic carbon (net community production). Figure 8 shows the annual cycling of vertically

integrated POC and DOC onshore flux at 25 km distance from the coast together with the net dissolved inorganic carbon (DIC) production in the near-coast waters up to that location.

[Figure 8 about here.]

Particulate carbon is transported towards the coast mainly during summer when the POC concentration is high and density gradients are strongest. The DOC flux is comparibly weak and directed towards the coast, which is associated with hydrolysis of near-bottom POC. For the given water volume, the net DIC production amounts to a similar carbon mass as transported towards the coast by estuarine circulation.

Depending on the burial of refractory POC, that is not subject to quick transformation into DIC in the upper sediments, the near-coast waters are potentially a DIC source, while the offshore waters potentially take up DIC from the atmosphere.

Given the annual increase of 0.11 t-C per meter coast line per year, a shelf sea with 1000 km coastline is expected to transport 0.009 Pmol-C per year towards its coasts. In the North Sea with approximately 1000 km coastline with continental Europe, this is approximately 10 % of the POC flux into the North Sea sediments as budgeted by Thomas et al. (2005). The flux analysis cannot provide a closed coastal carbon budget, but estimates the contribution of coastal transport processes to the carbon budget for the given hydrodynamical and ecosystem conditions.

3.5. Atmospheric deposition, sinking velocity and precipitation

Atmospheric deposition alone could be a key process for explaining the nutrient gradients without circulation effects. Additionally, an increased density gradient through increased precipitation and an increased sinking velocity of detritus could potentially enhance gradients in the system. Sensitivity studies on boundary nutrient fluxes, sinking velocity and precipitation can be found in figures 9 to 11. The increasing deposition as a surface flux of nutrients goes together with increasing lateral nutrient gradients. In the sensitivity studies, we use a deposition of 500 mg-N m^2 y^{-1} (Dentener et al. (2006)), which counteracts to denitrification in the sediments of the same order of magnitude for the Wadden Sea (Deek et al. (2013) found denitrification rates below 4 muM-N/m2/h which is an equivalent amount of 491 mg-N m^2 y^{-1} for their stations far from the Elbe mouth). The variability of the horizontal gradient associated with a domain-wide, net vertical boundary flux due to deposition and sediment fluxes is evaluated in figure 9.

[Figure 9 about here.]

In the deposition analysis, we assume, that boundary fluxes are potentially balanced since both, dissolved inorganic silicate and nitrogen show horizontal gradients (compare figure 5). The boundary flux is therefore artificially varied for ±25 % and ±50 % of the estimated 500 mg-N m^2 y^{-1} and applied as surface DIN flux. The negative fluxes are limited in case of depleted nutrients. The nutrient gradients in the transect

respond linearly to the imposed forcing for the linearly varying bathymetry and horizontally homogeneous boundary fluxes. The system's reaction suggests, that primary production is homogeneously limited by either light (in early spring and late summer) or nutrients (in late spring) along the idealised transect. A more non-linear response is expected for variable bathymetry and constricted, shallow embayments. Similarly, the responses on variation of the sinking velocity as of the precipitation increase the horizontal gradients for increased precipitation and sinking velocities (CITE JOERAN). The quantitative results of the simple variational analysis presented here would certainly change substantially with the environmental setup. The qualitative results suggest an implicit control of simulated coastal eutrophication based on uncertain model parameterisation as diffuse fresh water fluxes and sinking of fractal, organic particles.

[Figure 10 about here.]

[Figure 11 about here.]

4. summary & conclusions

The biogeochemical system in a cross-shore transect is simulated with a fully coupled model system of ocean physics, suspended particulate matter and carbon and nitrogen resolving ecosystem model in simplified two-dimensional model setup. The simple approach of the model setup allowed to study processes in coastal system independent of local coastlines, bathymetries and lateral forcing. We found that, the coastal freshwater budget has a significant influence on the nutrient cycles, such that forcing of rain and river inputs determine simulated nutrient gradients in coastal systems. In order to simulate coastal systems, the vertical resolution of the tidal mixing asymmetry is necessary in order to resolve the coastal matter fluxes associated with estuarine circulation. The sinking velocity of particulate organic matter is a major control for the accumulation of nutrients at the coast. A rough budget extrapolation shows, that the carbon transport towards the coasts may amount to 10 % of the carbon fluxes into the deeper sediments of a shelf sea, such as the North Sea. Eutrophication of a coastal system depends also on the eutrophication status of the open sea, since organic matter is transported from the deep water body towards the coasts. It remains unclear from the present results, how fast the coastal biogeochemical system would react on the long-term reduction of the open sea nutrient budget and which major feedbacks are expected.

5. Acknowledgements

The work of Richard Hofmeister has be funded by the Lower Saxony ministries for science and culture (MWK) and the ministry of Environment, Energy and Environmental Protection (MU) through the project WIMO. We want to thank Karsten Bolding and Jorn Bruggemann for maintaining the open-source modelling software FABM, GOTM and GETM.

References

Becherer, J., Burchard, H., Flöser, G., Mohrholz, V., Umlauf, L., Sep. 2011. Evidence of tidal straining in well-mixed channel flow from micro-structure observations. Geophysical Research Letters 38 (17), n/a–n/a.
URL http://doi.wiley.com/10.1029/2011GL049005

Bruggeman, J., Bolding, K., 2014. A general framework for aquatic biogeochemical models. Environm. Mod. & Software 61, 249–265.

Burchard, H., Bolding, K., Villarreal, M. R., 2004. Three-dimensional modelling of estuarine turbidity maxima in a tidal estuary. Ocean Dynamics 54, 250–265.

Burchard, H., Flöser, G., Staneva, J. V., Badewien, T. H., Riethmüller, R., Mar. 2008. Impact of Density Gradients on Net Sediment Transport into the Wadden Sea. Journal of Physical Oceanography 38 (3), 566–587.
URL http://journals.ametsoc.org/doi/abs/10.1175/2007JPO3796.1

Burchard, H., Hetland, R. D., Jun. 2010. Quantifying the Contributions of Tidal Straining and Gravitational Circulation to Residual Circulation in Periodically Stratified Tidal Estuaries. Journal of Physical Oceanography 40 (6), 1243–1262.
URL http://journals.ametsoc.org/doi/abs/10.1175/2010JPO4270.1

Burnett, W. C., Bokuniewicz, H., Huettel, M., Moore, W. S., Taniguchi, M., Nov. 2003. Groundwater and pore water inputs to the coastal zone. Biogeochemistry 66 (1/2), 3–33.
URL http://link.springer.com/10.1023/B:BIOG.0000006066.21240.53

Cloern, J. E., 1987. Turbidity as a control on phytoplankton biomass and productivity in estuaries. Cont. Shelf Res. 7, 1367–1381.

Deek, a., Dähnke, K., van Beusekom, J., Meyer, S., Voss, M., Emeis, K., Nov. 2013. N2 fluxes in sediments of the Elbe Estuary and adjacent coastal zones. Marine Ecology Progress Series 493, 9–21.
URL http://www.int-res.com/abstracts/meps/v493/p9-21/

Delaney, M. L., Dec. 1998. Phosphorus accumulation in marine sediments and the oceanic phosphorus cycle. Global Biogeochemical Cycles 12 (4), 563–572.
URL http://doi.wiley.com/10.1029/98GB02263

Dentener, F., Drevet, J., Lamarque, J. F., Bey, I., Eickhout, B., Fiore, a. M., Hauglustaine, D., Horowitz, L. W., Krol, M., Kulshrestha, U. C., Lawrence, M., Galy-Lacaux, C., Rast, S., Shindell, D., Stevenson, D., Van Noije, T., Atherton, C., Bell, N., Bergman, D., Butler, T., Cofala, J., Collins, B., Doherty, R., Ellingsen, K., Galloway, J., Gauss, M., Montanaro, V., Müller, J. F., Pitari, G., Rodriguez, J., Sanderson, M., Solmon, F., Strahan, S., Schultz, M., Sudo, K., Szopa, S., Wild, O., Dec. 2006. Nitrogen and sulfur deposition on regional and global scales: A multimodel evaluation. Global Biogeochemical Cycles 20.
URL http://doi.wiley.com/10.1029/2005GB002672

Ebenhöh, W., Kohlmeier, C., Baretta, J., Flöser, G., May 2004. Shallowness may be a major factor generating nutrient gradients in the Wadden Sea. Ecological Modelling 174 (3), 241–252.
URL http://linkinghub.elsevier.com/retrieve/pii/S0304380003004277

Engel, A., Thoms, S., Riebesell, U., Rochelle-Newall, E., Zondervan, I., 2004. Polysaccharide aggregation as a potential sink of marine dissolved organic carbon. Nature 428 (6986), 929–932.

Feser, F., Weisse, R., von Storch, H., 2001. Multi-decadal atmospheric modeling for Europe yields multi-purpose data. Eos, Transactions American Geophysical Union 82 (28), 305–310.

Fettweis, M., Francken, F., Van den Eynde, D., Verwaest, T., Janssens, J., Van Lancker, V., 2010. Storm influence on SPM concentrations in a coastal turbidity maximum area with high anthropogenic impact (southern North Sea). Continental Shelf Research 30 (13), 1417–1427.
URL http://dx.doi.org/10.1016/j.csr.2010.05.001

Flöser, G., Riethmüller, R., Nauw, J., Burchard, H., 2013. Observational evidence for the general presence of estuarine circulation in the Wadden Sea. Journal of Coastal Research 65, 1527–1532.

Frank, C., Schroeder, F., Ebinghaus, R., Ruck, W., 2006. A Fast Sequential Injection System for the Simultaneous Determination of Ammonia and Phosphate. Microchimica Acta 154, 31–38.

Gayer, G., Dick, S., Pleskachevsky, A., Rosenthal, W., Mar. 2006. Numerical modeling of suspended matter transport in the North Sea. Ocean Dynamics 56 (1), 62–77.
URL http://link.springer.com/10.1007/s10236-006-0070-5

Geider, R. J., Maclntyre, H. L., Kana, T. M., 1998. A dynamic regulatory model of phytoplanktonic acclimation to light, nutrients, and temperature. Limnology and Oceanography 43 (4), 679–694.

Geyer, W. R., MacCready, P., Jan. 2014. The Estuarine Circulation. Annual Review of Fluid Mechanics 46 (1), 175–197.
URL http://www.annualreviews.org/doi/abs/10.1146/annurev-fluid-010313-141302

Grasshoff, K., Ehrhardt, M., Kremling, K., 1999. Methods of Seawater Analysis, third edit Edition. Wiley-VCh, New York.

Gräwe, U., Wolff, J.-O., Ribbe, J., Jan. 2010. Impact of climate variability on an east Australian bay. Estuarine, Coastal and Shelf Science 86 (2), 247–257.
URL http://linkinghub.elsevier.com/retrieve/pii/S0272771409005356

Grunwald, M., Dellwig, O., Kohlmeier, C., Kowalski, N., Beck, M., Badewien, T. H., Kotzur, S., Liebezeit, G., Brumsack, H.-J., Oct. 2010. Nutrient dynamics in a back barrier tidal basin of the Southern North Sea: Time-series, model simulations, and budget estimates. Journal of Sea Research 64 (3), 199–212.

Hetzel, Y., Pattiaratchi, C., Lowe, R., Sep. 2013. Intermittent dense water outflows under variable tidal forcing in Shark Bay, Western Australia. Continental Shelf Research 66, 36–48.
URL http://linkinghub.elsevier.com/retrieve/pii/S0278434313002161

Jay, D. a., Musiak, J. D., 1994. Particle trapping in estuarine tidal flows. Journal of Geophysical Research 99 (C10), 20445.
URL http://doi.wiley.com/10.1029/94JC00971
Lucotte, M., D'Anglejan, B., 1983. Forms of phosphorus and phosphorus-iron relationships in the suspended matter of the St . Lawrence Estuary. Canadian Journal of Earth Science 20, 1880–1890.
Onken, R., Riethmüller, R., May 2010. Determination of the freshwater budget of tidal flats from measurements near a tidal inlet. Continental Shelf Research 30 (8), 924–933.
URL http://linkinghub.elsevier.com/retrieve/pii/S0278434310000403
Pritchard, D., a.J. Hogg, 2003. Cross-shore sediment transport and the equilibrium morphology of mudflats under tidal currents 108, 1–15.
URL http://dx.doi.org/10.1029/2002JC001570
Puls, W., Bernem, K.-H., Eppel, D., Kapitza, H., Pleskachevsky, A., Riethmüller, R., Vaessen, B., Sep. 2011. Prediction of benthic community structure from environmental variables in a soft-sediment tidal basin (North Sea). Helgoland Marine Research 66 (3), 345–361.
Schartau, M., Engel, A., Schröter, J., Thoms, S., Völker, C., Wolf-Gladrow, D., 2007. Modelling carbon overconsumption and the formation of extracellular particulate organic carbon. Biogeosciences Discussions 4 (1), 13–67.
Simpson, J. H., Brown, J., Matthews, J., Allen, G., Jun. 1990. Tidal Straining, Density Currents, and Stirring in the Control of Estuarine Stratification. Estuaries 13 (2), 125.
URL http://link.springer.com/10.2307/1351581
Soulsby, R. L., 1997. Dynamics of Marine Sands. Thomas Telford, London.
Stacey, M. T., Brennan, M. L., Burau, J. R., Monismith, S. G., Nov. 2010. The Tidally Averaged Momentum Balance in a Partially and Periodically Stratified Estuary. Journal of Physical Oceanography 40 (11), 2418–2434.
URL http://journals.ametsoc.org/doi/abs/10.1175/2010JPO4389.1
Stanev, E. V., Dobrynin, M., Pleskachevsky, A., Grayek, S., Günther, H., Dec. 2008. Bed shear stress in the southern North Sea as an important driver for suspended sediment dynamics. Ocean Dynamics 59 (2), 183–194.
URL http://link.springer.com/10.1007/s10236-008-0171-4
Thomas, H., Bozec, Y., de Baar, H. J. W., Elkalay, K., Frankignoulle, M., Schiettecatte, L.-S., Kattner, G., Borges, a. V., 2005. The carbon budget of the North Sea. Biogeosciences 2 (1), 87–96.
van Beusekom, J., Loebl, M., Martens, P., Jan. 2009. Distant riverine nutrient supply and local temperature drive the long-term phytoplankton development in a temperate coastal basin. Journal of Sea Research 61 (1-2), 26–33.
URL http://linkinghub.elsevier.com/retrieve/pii/S1385110108000531
van der Molen, J., Bolding, K., Greenwood, N., Mills, D. K., Mar. 2009. A 1-D vertical multiple grain size model of suspended particulate matter in combined currents and waves in shelf seas. Journal of Geophysical Research 114 (F1), 1–15.
URL http://www.agu.org/pubs/crossref/2009/2008JF001150.shtml
Van Engeland, T., Soetaert, K., Knuijt, A., Laane, R., Middelburg, J., Sep. 2010. Dissolved organic nitrogen dynamics in the North Sea: A time series analysis (1995-2005). Estuarine, Coastal and Shelf Science 89 (1), 31–42.
URL http://linkinghub.elsevier.com/retrieve/pii/S0272771410001964
Wu, Z., Zhou, H., Zhang, S., Liu, Y., Aug. 2013. Using 222Rn to estimate submarine groundwater discharge (SGD) and the associated nutrient fluxes into Xiangshan Bay, East China Sea. Marine pollution bulletin 73 (1), 183–91.
URL http://www.ncbi.nlm.nih.gov/pubmed/23790526

List of Figures

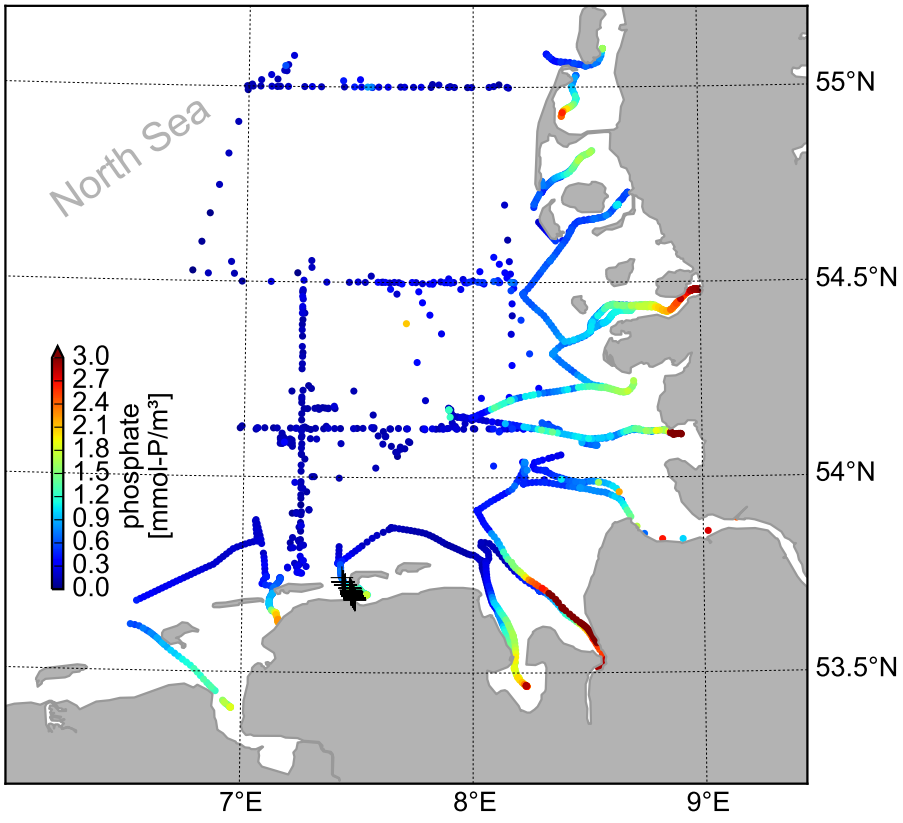

Figure 1: Map of German Bight and phosphate concentrations measured during a field experiment in summer 2005 with two research vessels. The measurements close to the mainland were performed during low tide. The black crossmarks at around 7.4°E,53.7°N give the locations of nutrient measurements in 2003.

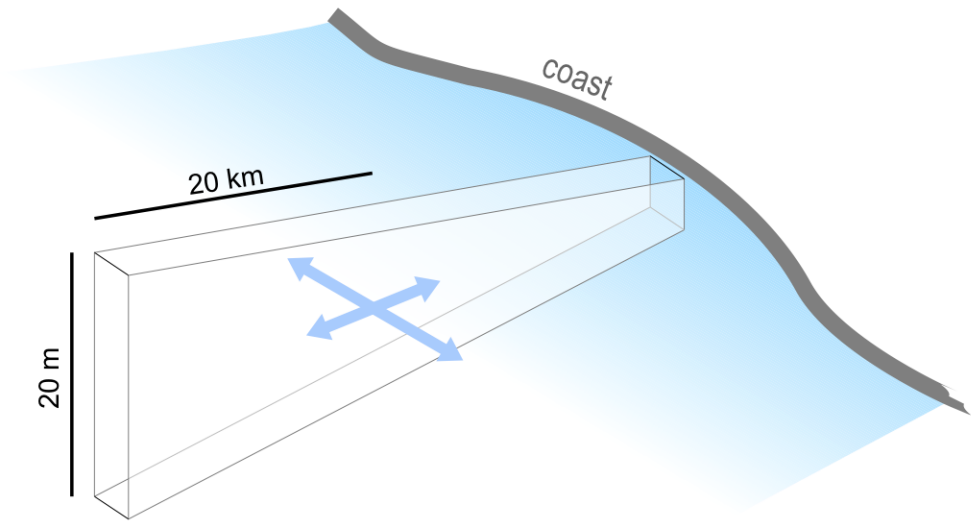

Figure 2: Schematic layout of the model setup. The vertical transect assumes zero-gradient conditions across the transect, while transports accelerated by wind or coriolis force are allowed. hydrodynamical processes along the transect are fully resolved in the numerical model.

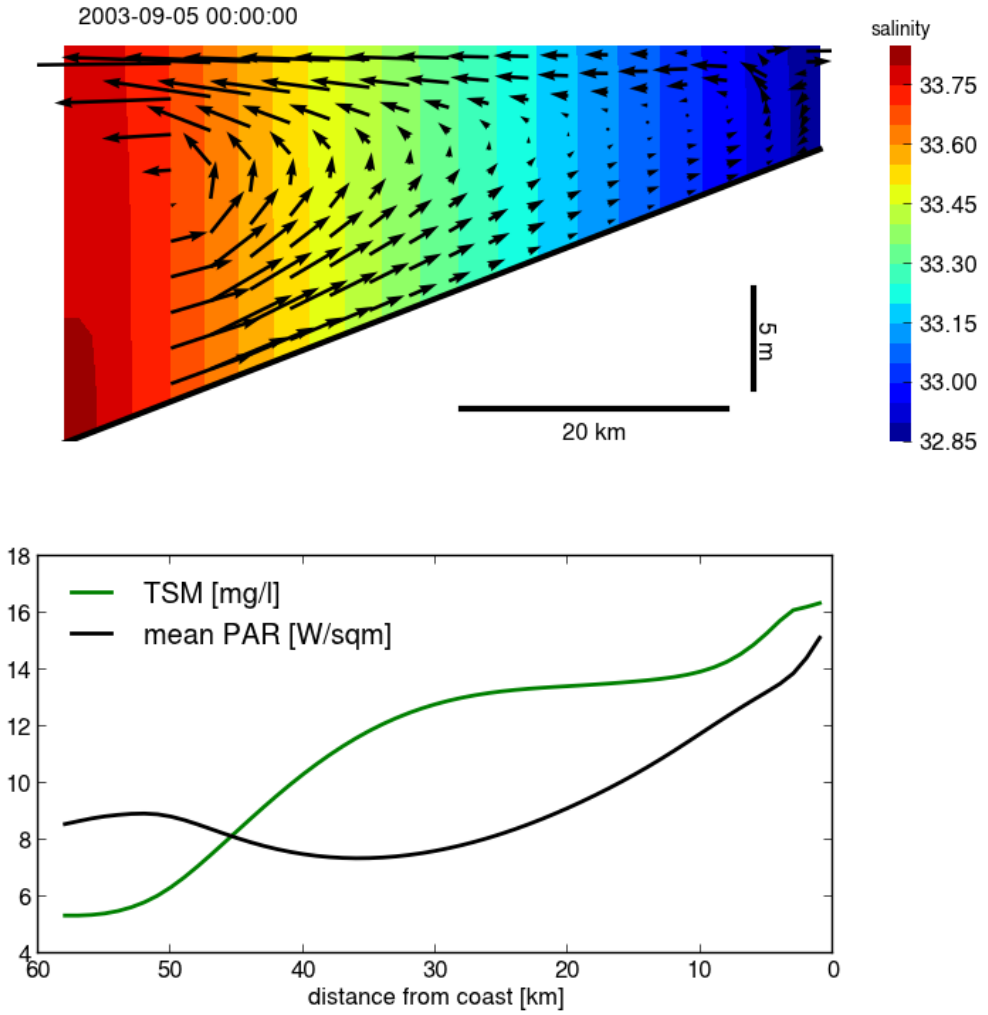

Figure 3: Tidally mean salinity and flow velocities for the realistic humid forcing in September in the upper panel. The corresponding total suspended matter concentration (TSM) and the vertically averaged available light field (mean PAR) in the lower panel.

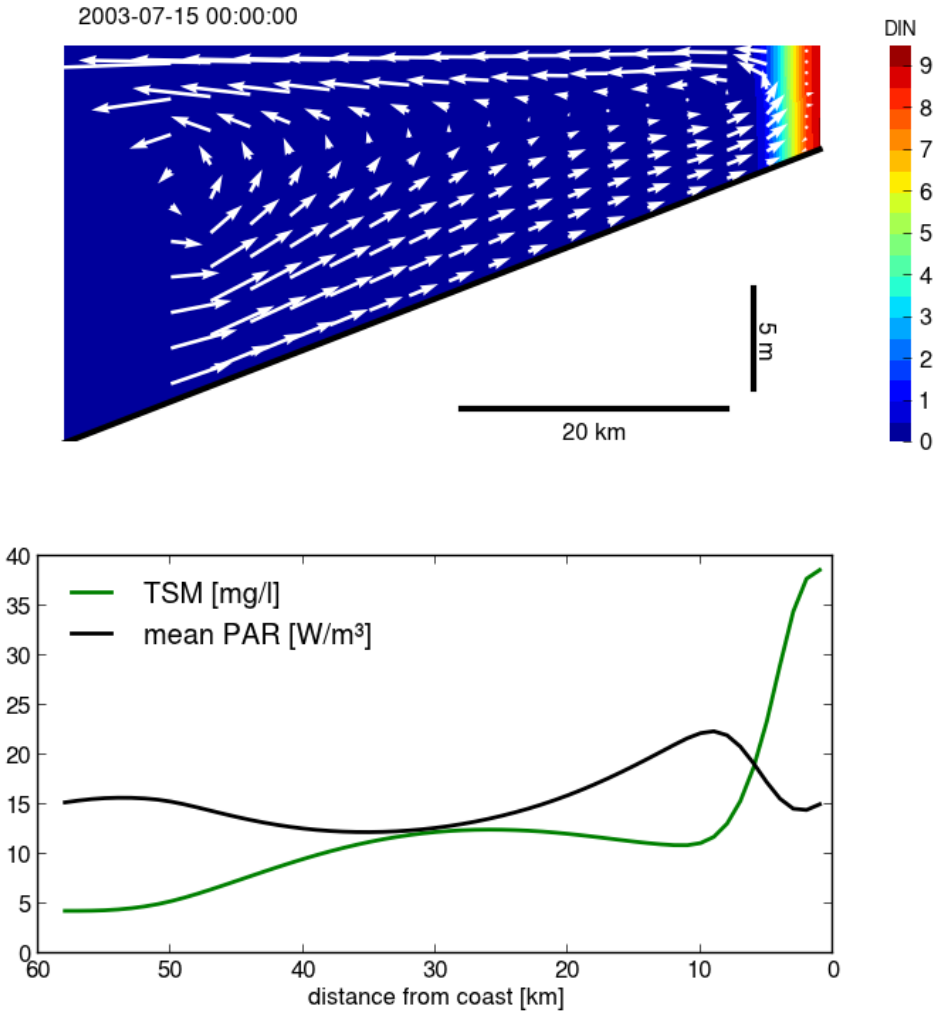

Figure 4: Tidally mean nutrient gradients and the flow velocities for the realistic humid forcing in July in the upper panel. The corresponding total suspended matter concentration (TSM) and the vertically averaged available light field (mean PAR) in the lower panel.

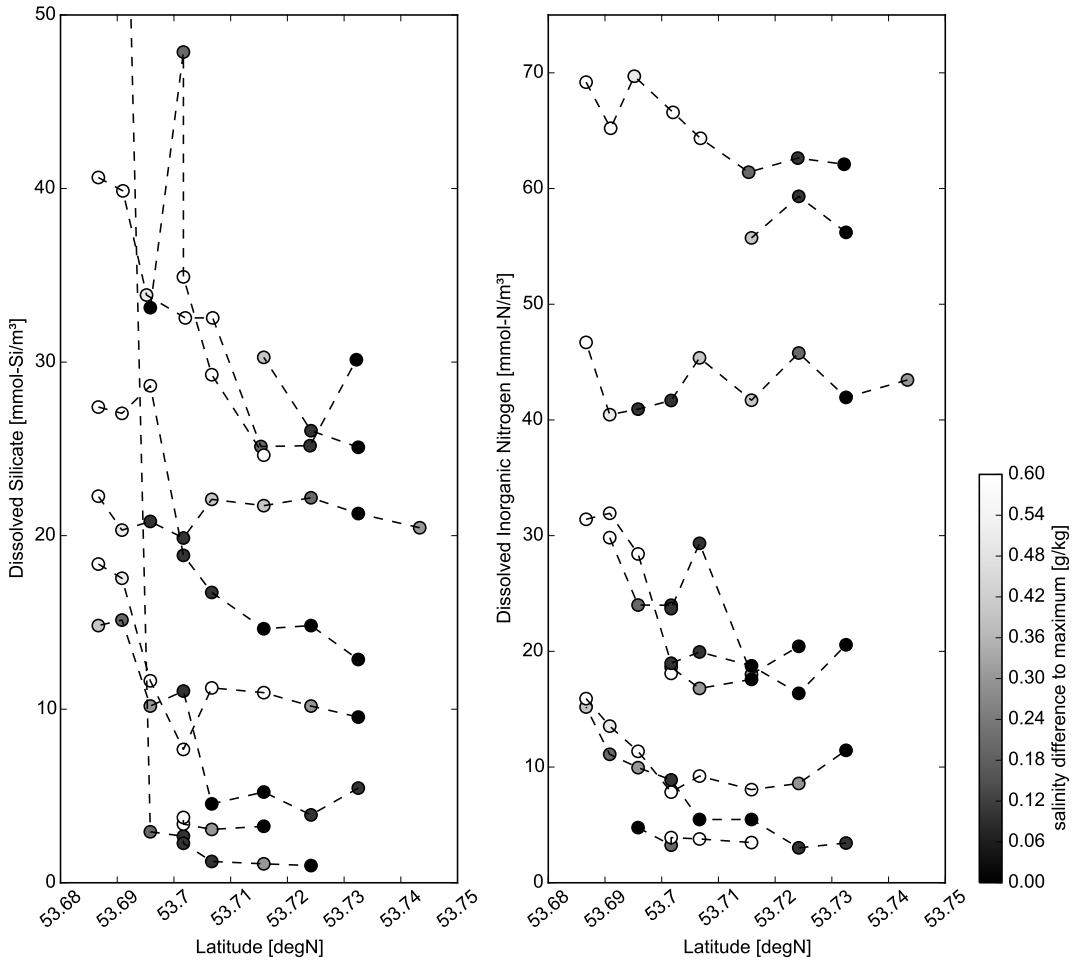

Figure 5: DIN and Silicate cross-shore profiles measured in the East Frisian Wadden Sea (see figure 5 for the location) and shown for profiles with an observed salinity gradient, as given by the colouring of the circles.

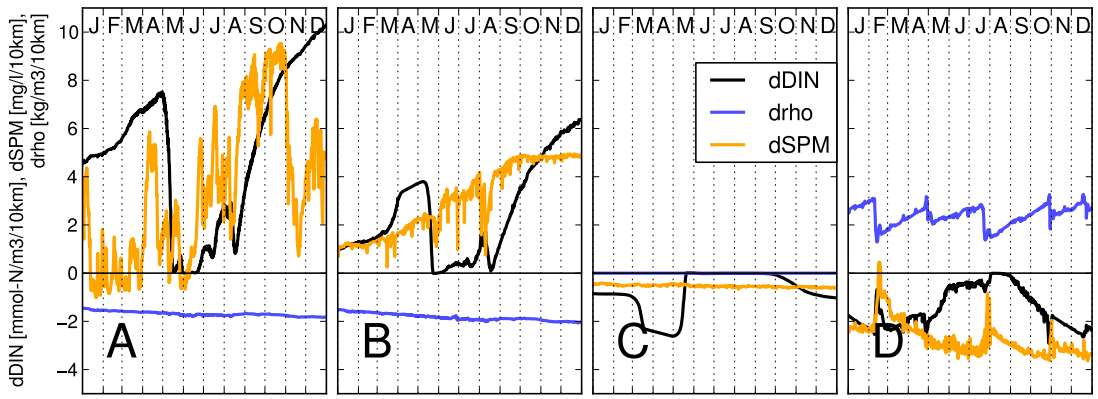

Figure 6: Nutrient and suspended matter concentration increase per 10 km towards the coast and the 10-fold density increase per 10 km for idealised humid forcing (A), realistic humid forcing (B), artifically vanished density gradient (C) and an idealised arid forcing (D)

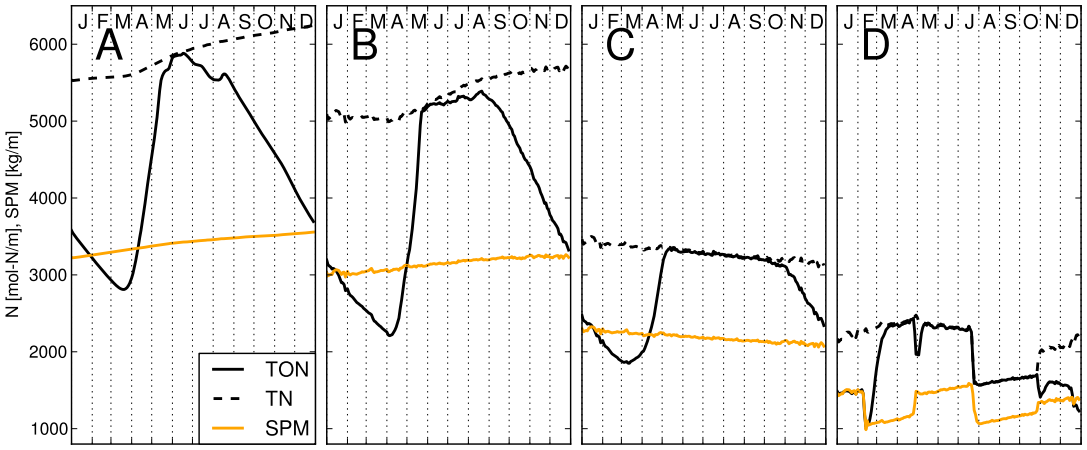

Figure 7: Total organic nitrogen (TON), total nitrogen (TN) and suspended particular matter (SPM) for idealised humid forcing (A), realistic humid forcing (B), an artificially vanished density gradient (C), and an inverse estuary (D)

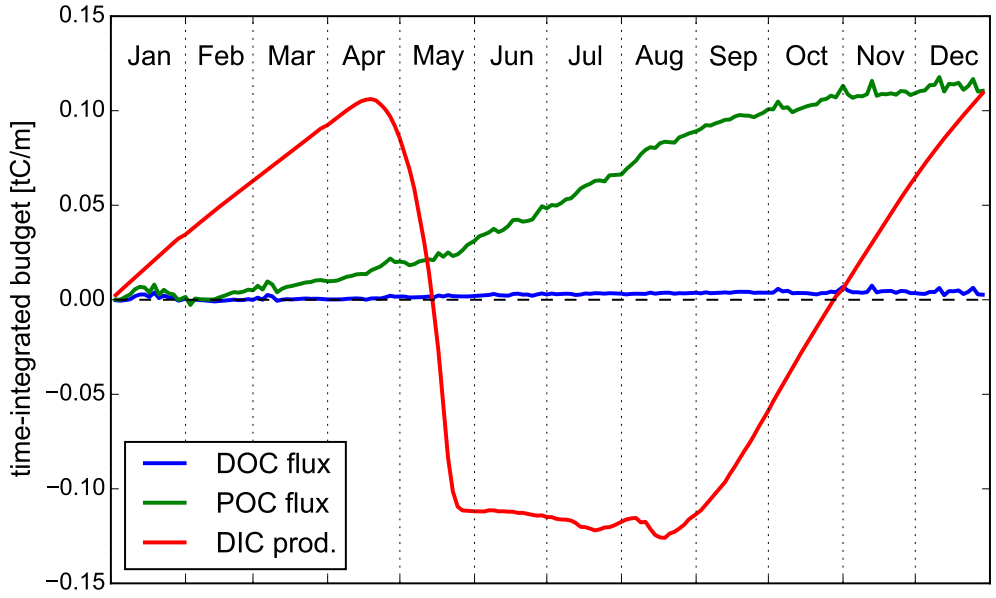

Figure 8: temporally integrated budget of vertically integrated, horizontal flux of dissolved organic carbon (DOC flux) and particulate organic carbon (POC flux) at 25 km distance from the coast, and the horizontally and vertically integrated net DIC production up to 25 km distance from the coast for scenario B

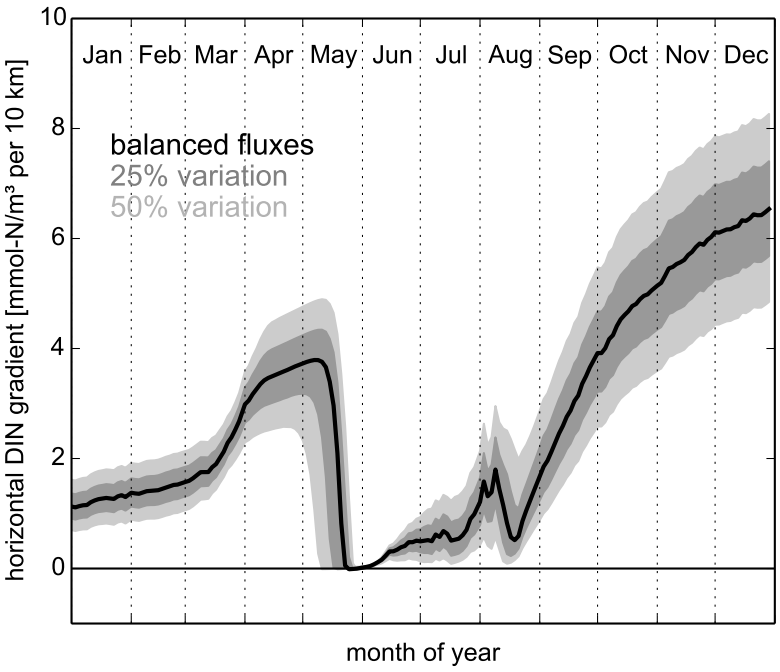

Figure 9: climatological nutrient gradient for different atmospheric depositions

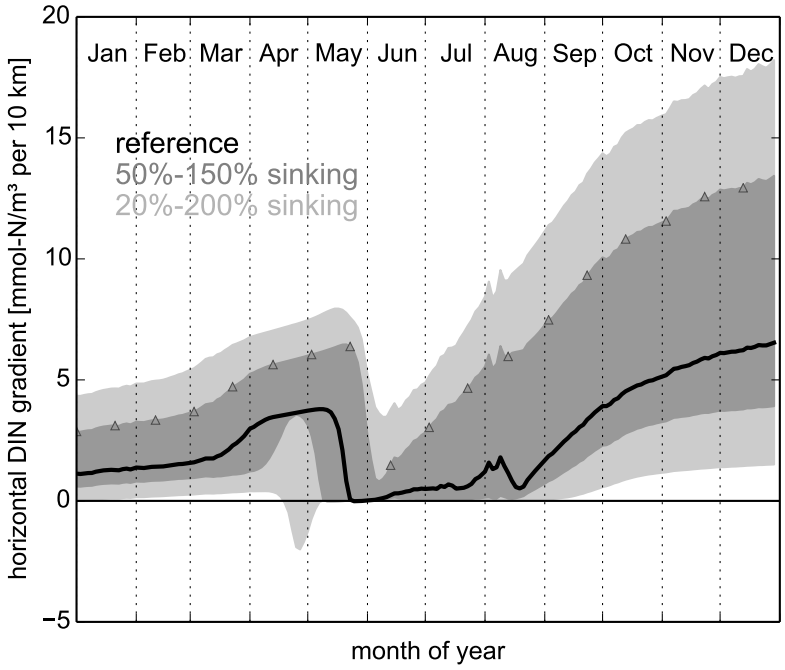

Figure 10: climatological nutrient gradient for different sinking velocities of particulate organic matter. The triangles indicate the upper boundary of the parameter variation.

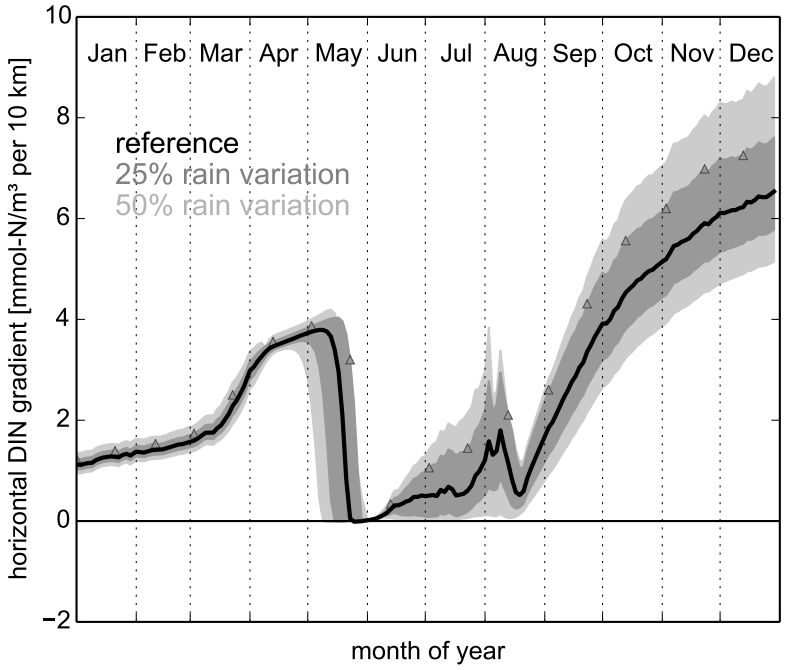

Figure 11: climatological nutrient gradient for different fresh water fluxes due to precipitation. The triangles indicate the upper boundary of the parameter variation.

List of Tables

parameter	description	value	unit
w_s^{SPM}	sinking velocity of SPM	2	m d^{-1}
k_d^{SPM}	shading parameter for SPM	0.1	l mg^{-1} m^{-1}
k_d^{PON}	shading parameter for PON	0.01	m^2 $mmolN^{-1}$
k_d^0	background shading parameter	0.3	m^{-1}
A_e	activation energy	4500.	
T_{ref}	reference temperature	13	°C
P_{max}	maximum growth rate	2.3	d^{-1}
α	initial slope of PI-curve	0.3	m^2 molC μE^{-1} $gChl^{-1}$
ζ_{CN}	respiratory costs NO_3 reduction	2.3	molC $molN^{-1}$
$Chl{:}N_{max}$	maximum CHL:N ratio	4.2	gChl $molN^{-1}$
l_{phy}^N	phytoplankton N loss	0.018	d^{-1}
l_{phy}^C	phytoplankton C loss	0.025	d^{-1}
Q_0^N	subsistence N:C ratio	0.043	molN $molC^{-1}$
Q_{max}^N	upper limit of N:C ratio	0.151	molN $molC^{-1}$
V_{NC}	maximum nutrient uptake	0.7	d^{-1}
k_N	half-saturation nutrients	1.0	mmolN m^{-3}
ϕ_{PD}	aggregation rate phytoplankton-detritus	0.02	m^3 $mmolN^{-1}$ d^{-1}
ϕ_{PP}	aggregation rate phytoplankton-phytoplankton	0.02	m^3 $mmolN^{-1}$ d^{-1}
w_s^{phy}	sinking velocity of phytopankton	1.0	m d^{-1}
w_s^{det}	sinking velocity of detritus	10.0	m d^{-1}
h_{PON}	PON hydrolysis rate	0.008	d^{-1}
h_{TEP}	TEP hydrolysis rate	0.01	d^{-1}
r	remineralisation rate	0.02	d^{-1}
g_{max}	maximum grazing rate	0.2	d^{-1}
k_{graz}	half-saturated grazing	1.0	mmolN m^{-3}
y_{zoo}	zooplankton yield factor	1.0	
l_{zoo}^{mort}	zooplankton quadratic mortality	0.1	m^3 $mmolN^{-1}$ d^{-1}
l_{zoo}^{resp}	zooplankton resporation loss	0.01	d^{-1}
Q_{zoo}	zooplankton N:C ratio	0.16	molN $molC^{-1}$

Table 1: Model parameters used in the ecosystem and SPM model